Identifying calcium-containing mineral species in the JEB Tailings Management Facility at McClean Lake, Saskatchewan

Peter E. R. Blanchard**, Andrew P. Grosvenor*

Department of Chemistry, University of Saskatchewan, Saskatoon, SK, S7N 5C9

John Rowson, Kebbi Hughes, Caitlin Brown

AREVA Resources Canada, Saskatoon, SK, S7K 3X5

*Author to whom correspondence should be addressed

E-mail: andrew.grosvenor@usask.ca

Phone: (306) 966-4660

Fax: (306) 966-4730

**Current address: Canadian Light Source, Saskatoon, SK S7N 2V3

Abstract

The JEB Tailings Management Facility (TMF) is central to reducing the environmental impact of the McClean Lake uranium mill facility that is operated by AREVA Resources Canada. This facility has been designed around the idea that elements of concern (e.g., U, As, Ni, Se, Mo) will be controlled through equilibrium with precipitants. Confirming the presence of calcium-containing carbonates in the JEB TMF is the first step in determining if gypsum ($CaSO_4 \cdot 2H_2O$) controls the concentration of HCO_3^- (aq), limiting the formation of soluble uranyl bicarbonate complexes. A combination of X-ray diffraction (XRD), X-ray absorption near-edge spectroscopy (XANES), and microprobe X-ray fluorescence (XRF) mapping was used to analyze a series of tailings samples from the JEB TMF. Calcium carbonate in the form of calcite ($CaCO_3$), aragonite ($CaCO_3$), and dolomite ($CaMg(CO_3)_2$) were identified by analysing Ca K-edge μ-XANES spectra coupled with microprobe XRF mapping. This is the first observation of these phases in the JEB TMF. The combination of μ-XANES and XRF mapping provided a greater sensitivity to low concentration calcium species compared to the other techniques used, which were only sensitive to the major species present (e.g., gypsum).

Keywords: Uranium mining; Calcium; tailings; synchrotron radiation; X-ray absorption spectroscopy; X-ray microprobe

1. Introduction

AREVA Resources Canada (AREVA) operates the JEB Tailings Management Facility (TMF) to manage and dispose of elements of concern generated in the U ore milling operations located at McClean Lake, Saskatchewan. A location map showing the JEB mill and TMF, as well as some of the ore bodies that feed the mill is presented in Figure S1 in the Supporting Information (SI). The JEB TMF is designed to reduce the migration of water-soluble elements that co-mineralize with U ore (i.e., As, Ni, Mo, and Se) by promoting the formation of water-insoluble mineral species, effectively "trapping" these elements of concern (AREVA, 2015). The concentration of the solutes are out of equilibrium with the desired mineral phases when initially added to the TMF and may require a long period of time to reach a stable mineralogical end-point. Mineralogical evolution is limited by low temperatures (+6 ^{o}C), low hydraulic conductivity, and low liquid/solid ratios that reduces mass transport (AREVA, 2015). A table that identifies a selection of the primary and secondary minerals present in the tailings before being placed in the TMF can be found in the SI (Table S1).

AREVA has been investigating the long-term formation of solid phases containing several elements of concern in the TMF (e.g., As, Ni, Mo) (Langmuir et al., 2006; Mahoney et al., 2007; Chen et al., 2009; Hayes et al., 2014; Blanchard et al., 2015). However, there is little known about the behaviour of U in the JEB TMF. The process of separating yellow cake (U_3O_8(s)) from the ore consumes small amounts of hydrocarbon material. The largest sources of hydrocarbons used in the mill are organic flocculent (polyacrylamide) and kerosene. Small amounts of kerosene are lost to the raffinate solution that reports to the tailings preparation process. This hydrocarbon material adsorbs onto the surface of the tailings solids and is subsequently deposited in the TMF. Hydrocarbons in the tailings are gradually converted to

soluble HCO_3^-(aq) (bicarbonate) in the tailings pore water, which is facilitated by the presence of bacterial communities. Under the oxic conditions of the TMF (Eh ~ +290 mV; pH ~ 7), U oxide (e.g., UO_2, U_3O_8, $U(SiO_4)_{1-x}(OH)_{4x}$) in the tailings may react with bicarbonate to form an undesirable water-soluble uranyl-carbonate complex. Dissolved bicarbonate can be removed from the TMF pore water by co-precipitating with dissolved Ca^{2+}(aq) as calcium carbonate ($CaCO_3$(s)). The concentration of dissolved Ca^{2+}(aq) is relatively high in the TMF (~550 mg/L), as the TMF is saturated with gypsum ($CaSO_4 \cdot 2H_2O$(s)) that forms from the addition of sulfuric acid and lime during the leaching and tailings preparation stages, respectively. Overall, the conversion of gypsum to calcium carbonate (calcite or aragonite) can be written as (AREVA, 2015):

$$CaSO_4 \cdot 2H_2O(s) + HCO_3^-(aq) + OH^-(aq) \rightarrow CaCO_3(s) + SO_4^{2-}(aq) + 3H_2O(l) \quad (1)$$

Although there is some indirect evidence of calcium carbonate precipitation as observed by the decrease in concentration of Ca^{2+}(aq) in the pore water collected at lower elevations (i.e., deeper depths) of the TMF (AREVA, 2015), calcium carbonate has not been directly observed. Identifying calcium-containing carbonate is an essential first step to understanding how the HCO_3^-(aq) concentration is controlled in the TMF. Our recent X-ray diffraction (XRD), X-ray absorption near-edge spectroscopy (XANES), and X-ray fluorescence (XRF) microprobe studies have proven useful in identifying Mo-bearing mineral species in the TMF, particularly at low concentrations (Hayes et al., 2014; Blanchard et al., 2015). In the current study, the calcium mineralization in the JEB TMF has been investigated using a combination of these techniques. Detailed micro powder XRD and bulk XANES analyses indicated that the major Ca-containing mineral species in the TMF are gypsum and possibly anhydrite ($CaSO_4$). Micro XANES (μ-XANES) analysis was able to identify several minor calcium-containing mineral species,

including calcite, aragonite, and dolomite ($CaMg(CO_3)_2$). Overall, this investigation has demonstrated that μ-XANES coupled with XRF mapping is the most effective way to identify low concentration calcium species in the TMF.

2. Experimental

2.1 Tailings sample description

The samples studied were collected during the 2013 sampling campaign of the JEB TMF. Samples were collected from two borehole locations in the TMF. A total of six samples were provided for this study, with three samples collected from the central borehole (TMF13-01-SA12, TMF13-01-SA19, TMF13-01-SA22) and three samples from a periphery borehole (TMF13-03-SA12, TMF13-03-SA15, TMF13-03-SA19) located approximately 55 m from the centre. A figure showing a schematic of the TMF and the location of the bore-holes in plan view is shown in Figure S2 in the SI. The tailings are placed in the TMF using a floating barge and tremie piping system in a way that minimizes particle size segregation at the point of placement; however, it does not eliminate it. As a consequence, the particle size distribution of the tailings solids is not homogenous in the TMF with the central bore hole possessing a coarser particle size distribution than bore holes located at the periphery of the TMF. More information on the sampling of the tailings can be found in the SI.

2.2 Micro powder XRD

Micro powder X-ray diffraction (μ-XRD) patterns of the tailings samples were collected to determine which crystalline phases are present in the bulk material. Measurements were performed using a PANalytical Empyrean powder X-ray diffractometer equipped with a Cu $K\alpha_{1,2}$ X-ray source, and powder XRD patterns were analyzed using the PowderCell software package (Kraus and Nolze, 1996). Unground grains from each tailings sample was measured

instead of finely ground powder in an attempt to increase the possibility of detecting minor phases by μ-XRD. More information on these experiments can be found in the SI.

2.3 Bulk XANES

2.3.1 Bulk Ca K-edge XANES

Bulk Ca K-edge XANES measurements were collected on the Soft X-ray Microcharacterization Beamline (SXRMB; 06B1-1) at the CLS (Hu et al., 2010). Finely powdered (i.e., homogenized) tailings samples and standards were lightly dusted onto carbon tape mounted onto a multi-sample holder. A single layer of Kapton foil covered the tailings samples. More details on the experimental set-up can be found in the SI. All XANES spectra were analyzed using the Athena software program (Ravel and Newville, 2005). A quantitative analysis of the XANES spectra was performed using principle component analysis (PCA) followed by linear combination fitting (LCF) using the spectra from the standards The energy range used for PCA and LCF analysis was -20 and +40 eV relative to the Ca K-edge absorption edge energy.

2.3.2 Bulk Ca $L_{2,3}$-edge and C K-edge XANES

Bulk Ca $L_{2,3}$-edge and C K-edge XANES spectra from the tailings samples and standards were collected on the Spherical Grating Monochromator (SGM; 11ID-1) beamline at the Canadian Light Source (Regier et al., 2007). Finely ground tailing samples and standards (powders and liquids) were either dusted on carbon tape (Ca $L_{2,3}$-edge) or drop-coated on a gold-plated silicon wafer (C K-edge). More details on the experimental set-up can be found in the SI. A quantitative analysis of the Ca $L_{2,3}$-edge XANES spectra was performed using PCA followed by LCF. The energy range used for this analysis was -1 and +5 eV relative to the Ca L_3-edge

absorption edge energy. Quantitative analysis could not be performed on the C K-edge due to overlap of the K $L_{2,3}$-edge.

2.4 Microprobe XRF mapping and Ca K-edge μ-XANES

Microprobe X-ray fluorescence (XRF) maps and Ca K-edge micro XANES (μ-XANES) spectra were collected using the SXRMB beamline (Hu et al., 2010). Unground tailings samples were placed onto carbon tape on a multi-sample holder and covered by Kapton foil. As will be observed during the discussion of the bulk Ca K-edge XANES spectra, collecting spectra from finely powdered tailings samples only resulted in the dominant phases being detected. In the case of the XRF/μ-XANES experiments, unground grains of the tailings were studied so as to increase the possibility of identifying minor Ca-containing phases. A 10 μm spot size was used to collect the XRF maps and μ-XANES spectra. XRF maps were collected by rastering a 500 μm x 500 μm or 1000 μm x 1000 μm area using a 10 μm step size with a 1 s dwell time at a monochromatic X-ray energy of 4100 eV. The Ca K-edge μ-XANES spectra were collected using similar parameters used to collect the bulk Ca K-edge spectra. XRF maps were created and analysed using the SMAK software program and μ-XANES spectra were analyzed using the Athena software program (Ravel and Newville, 2005; Webb, 2011).

2.5 Electron microprobe

Electron microprobe analysis of the tailings samples was carried out using a Japan Electron Optics Laboratory (JEOL) 8600 Superprobe electron microprobe at an accelerating voltage of 15 keV. Tailings samples were mounted in an epoxy resin and the surface was polished using diamond paste. Backscattered electron images and WDS (wavelength dispersive X-ray spectroscopy) maps were collected from each C-coated sample at a magnification of 120X.

3. Results and discussion

3.1 Powder micro X-ray diffraction

Powder μ-XRD patterns were collected from several (unground) grains of each sample. The μ-XRD patterns collected from tailings sample TMF13-01-SA19 are shown in Figure 1. Patterns collected from the other tailings samples are shown in the SI (Figures S3–S7). Analysis of the μ-XRD patterns highlights the heterogeneous nature of the tailings samples. μ-XRD diffraction patterns only represent the composition of a few individual grains at most given the small spot size used during the μ-XRD experiments and the large grain size of the tailings (up to hundreds of micrometers in diameter). The width and intensity of the diffraction peaks were observed to vary from spot to spot, which is due to variations in crystallinity and preferred orientation effects. The most common calcium-containing mineral species identified in the μ-XRD pattern was gypsum (cf., Scan 1 in Figure 1). Several patterns provided support for the presence of powellite ($CaMoO_4$; cf., Scans 2, 3 and 4 in Figure 1), which has been confirmed to be present in the JEB TMF in previous XANES studies (Hayes, et al., 2014; Blanchard et al., 2015). A few peaks are marked as "?" in the μ-XRD patterns (Figure 1 and Figures S3, S6, and S7 in SI) as they remain unidentified.

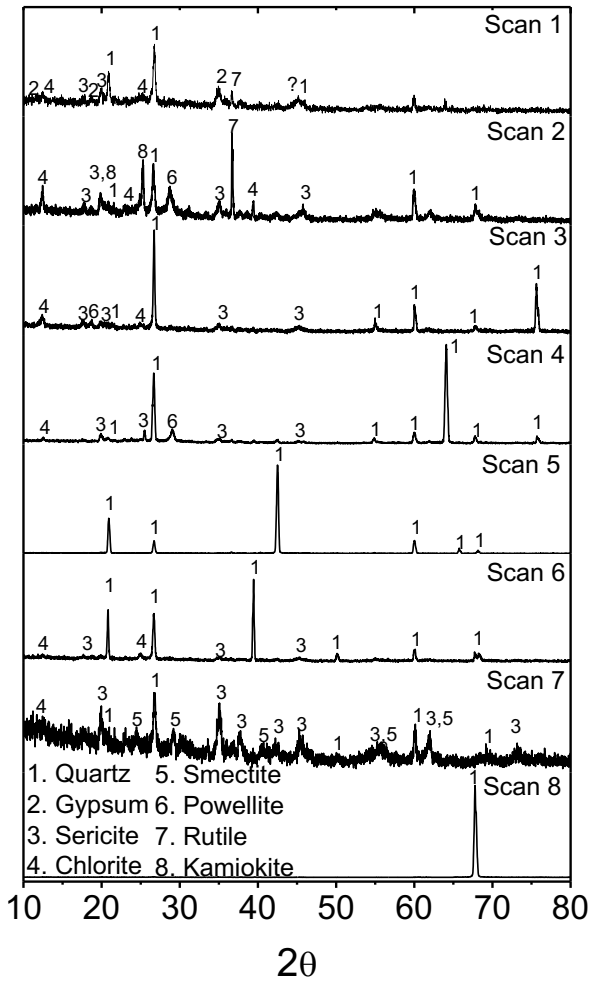

Figure 1. μ-XRD patterns collected from tailings sample TMF13-01-SA19. Evidence of gypsum is highlighted in scan 1 while evidence of powellite is highlighted in scan 3. The high 2θ diffraction peaks corresponding to quartz shown in the diffraction patterns collected in scans 4 and 8 are so intense due to preferred orientation effects.

3.2 Bulk XANES

Diffraction analysis identified quartz, gypsum, and various clay minerals as the major crystalline materials in the TMF (Hayes et al., 2014). The μ-XRD patterns also indicated that other calcium-containing mineral species might be present in the tailings samples, such as powellite. The presence of highly crystalline phases, particularly quartz, in the tailings likely impedes the ability of this technique to identify minor or poorly crystalline mineral species that may be present in the TMF. Our previous studies of Mo precipitation in the TMF have demonstrated that XANES is capable of detecting mineral species at low concentrations (i.e., ppm) in heterogeneous samples (Hayes et al., 2014; Blanchard et al., 2015). Bulk Ca K-edge and $L_{2,3}$-edge, and C K-edge XANES spectra of the tailings samples were collected from homogenized samples (i.e., finely ground) using a large (mm size) X-ray spot size.

3.2.1 Bulk Ca K-edge XANES

The bulk Ca K-edge XANES spectra of the tailings samples are shown in Figure 2a. The spectra from the tailings samples were compared to spectra from several calcium-containing standards, which are shown in Figure 2b. The Ca K-edge corresponds to a dipole-allowed transition of a 1s electron into unoccupied 4p states. The lineshape of the bulk Ca K-edge XANES spectrum is heavily dependent on the local coordination environment and is often analyzed to identify specific Ca-containing species present in a mixture (Sowrey et al., 2004; Takahashi et al., 2008; Liu et al., 2013). The bulk Ca K-edge XANES spectra from the tailings samples have similar lineshapes, suggesting that they consist of similar Ca-containing mineral species.

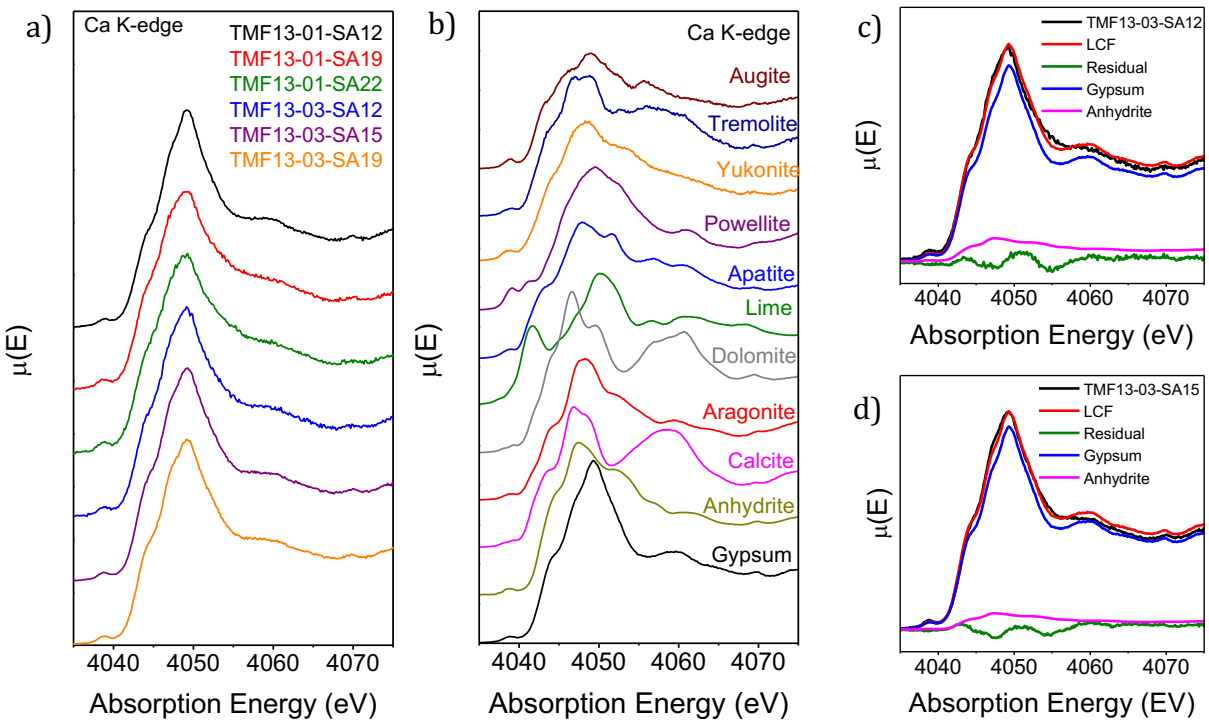

Figure 2. The Ca K-edge XANES spectra from the tailings and calcium-containing standards are shown in a) and b), respectively. The spectra from the tailings samples were all observed to have similar lineshapes. The fitted bulk Ca K-edge XANES spectra from TMF13-03-SA12 and TMF13-03-SA15 are shown in c) and d), respectively. The linear combination fitting of each spectrum is shown in red and the residual is shown in green. The weighted spectra from the standards used to fit the spectra from the tailings are also shown.

The PCA was used to determine the number of major calcium-containing mineral species present. Assuming a XANES spectrum consists of a linear combination of individual components of a mixture, a PCA calculation decomposes a series of spectra into a set of components (eigenvectors) and weightings (eigenvalues) that describe the variation in the data set (Fernández-Garcia et al., 1995; Beauchemin et al., 2002). Although these components are mathematical constructs with no simple relationship to the chemical species that make up the spectra, it has been assumed here that the minimum number of components that describe the variation in the data set is equivalent to the minimum number of chemical species that make up a XANES spectrum (Fernández-Garcia et al., 1995; Beauchemin et al., 2002). An indicator

function (IND) was developed by Malinowski to determine the minimum number of components required to describe a series of spectra (Malinowski, 2002; Malinowski, 1977). It is generally accepted that the minimum number of components is given when the IND function is minimized (Malinowski, 2002; Malinowski, 1977). The number of components predicted by the IND function can be tested by reconstructing the set of spectra using the components calculated in the PCA.

The PCA was performed on the six tailings samples, and the results are shown in Figure S8a in the SI. The first component calculated for each set of spectra accounts for >99 % of the total variances, which is common in PCA of XANES spectra (Cassinelli et al., 2014). The second component is the only other component with an observable intensity, suggesting that two components are required to describe the variation in the set of spectra studied. This was confirmed by calculating the IND value (see Figure S8b), which is at a minimum when the number of components equals two. Reconstructions of the spectrum of tailings sample TMF13-03-SA12 (Figure S9 in the SI) shows no visible improvements when reproducing the spectrum with two or three components.

The LCF analysis was used to identify the calcium-containing mineral species in the tailings samples. Each normalized bulk Ca K-edge spectrum was fitted by a linear combination of weighted standard spectra. The coefficients calculated in the LCF correspond to the concentration of each Ca species present. Based on the PCA calculations, the number of components used in the fittings was initially restricted to two. Best fits were determined by comparing the χ^2 value. The smaller the χ^2 value, the better the fit. Results of the best fits are tabulated in Table 1 and the fitted bulk Ca K-edge XANES spectra are shown in Figure 2c-d and Figure S10 in the SI. The best fits were obtained when fitting the spectra with two different

forms of calcium sulfate: gypsum and anhydrite. The majority of calcium in the tailings samples was gypsum, with concentrations ranging from 76–98 at%, while the concentration of anhydrite ranged from 2–24 at% (Table 1). The identification of anhydrite in the tailings might be due to local heating of the sample by the X-ray beam, resulting in dehydration of gypsum to anhydrite. This being said, the comparison of multiple spectra collected from the same spot did not show any appreciable differences, which is supportive of the finding of anhydrite in the tailings. Further, the spectrum from the gypsum standard did not change during data collection.

Misfits of the spectra are noticeable at higher absorption energies (4055–4070 eV). This region of a XANES spectrum is known to have contributions from multiple scattering resonances (MSR), a low-energy extended X-ray absorption fine structure (EXAFS) phenomenon that is highly dependent on the crystal structure and crystallinity (Rehr, 2000). The fittings in this region of the Ca K-edge suggests that the calcium-containing mineral species in the tailings may be of a lower crystallinity than the standards used in the LCF.

Table 1. Results of the LCF fitting of the bulk Ca K-edge XANES spectra from the tailings samples. Calculated errors are in brackets.

Sample	Gypsum (at%)	Anhydrite (at%)	R-factor	χ^2
TMF13-01-SA12	98(2)	2(2)	0.00581	0.409
TMF13-01-SA19	76(3)	24(3)	0.00627	0.506
TMF13-01-SA22	84(3)	16(3)	0.00674	0.535
TMF13-03-SA12	89(2)	11(2)	0.00487	0.330
TMF13-03-SA15	92(2)	8(2)	0.00451	0.323
TMF13-03-SA19	93(2)	7(2)	0.00312	0.226

3.2.2 Bulk Ca $L_{2,3}$-edge XANES

Information on the major Ca-containing mineral species can also be obtained from the Ca $L_{2,3}$-edge XANES spectra collected from homogenized tailings samples using a large X-ray spot size, and are shown in Figure 3a. The Ca L-edge splits by spin-orbit coupling, resulting in two features corresponding to dipole-allowed $2p_{3/2} \rightarrow 3d$ (L_3-edge) and $2p_{1/2} \rightarrow 3d$ (L_2-edge) transitions. The L_3- and L_2-edge further splits into two major peaks; labelled A and B for the L_3-edge and A` and B` for the L_2-edge. This splitting is characteristic of Ca^{2+} and loosely corresponds to the crystal field splitting of the Ca 3d states (Himpsel et al., 1991; Politi et al., 2005). The relative intensity and energy difference of features A (A`) and B (B`) depends on the local coordination environment of the Ca^{2+} cation. Several low intensity features are observed below 349 eV and are attributed to core-hole effects (De Groot et al., 1990). As can be observed by comparing the spectra from the tailings to the spectra from the standards in Figure 3b, the spectra from the tailings all have a similar lineshape to that of gypsum (cf. Figure 3c). This observation is consistent with the bulk Ca K-edge XANES analysis presented above. Note that feature B (B`) in the bulk Ca L_3(L_2)-edge spectra (see Figures 3c and 4) is more intense in the tailings samples than gypsum, possibly indicating the presence of other calcium-containing minerals.

The PCA analysis indicated that two components are required to explain the variation in the bulk Ca $L_{2,3}$-edge XANES spectra of the tailings samples (see Figure S11 in the SI). The LCF analysis of the Ca $L_{2,3}$-edge was then performed to determine the major calcium-containing mineral species in the tailings. Results of the LCF analysis are shown in Table 2 and the fitted bulk Ca $L_{2,3}$-edge XANES spectra are shown in Figure 4 when both gypsum and lime were used as the components. The LCF analysis indicated that gypsum was the major calcium-containing

mineral species in the tailings samples with the samples containing between 87% and 91% gypsum; however, it was not obvious from the LCF what minor calcium-containing minerals were present in the tailings samples. Fittings having similar R-factors and χ^2 values were obtained when fitting the spectra to gypsum and other calcium-containing standards, including lime, powellite, aragonite, calcite, and yukonite (cf. Figure 4 and Figure S12 in the SI). It is possible that crystallinity may affect the lineshape of the Ca $L_{2,3}$-edge, which would influence the results of the LCF.

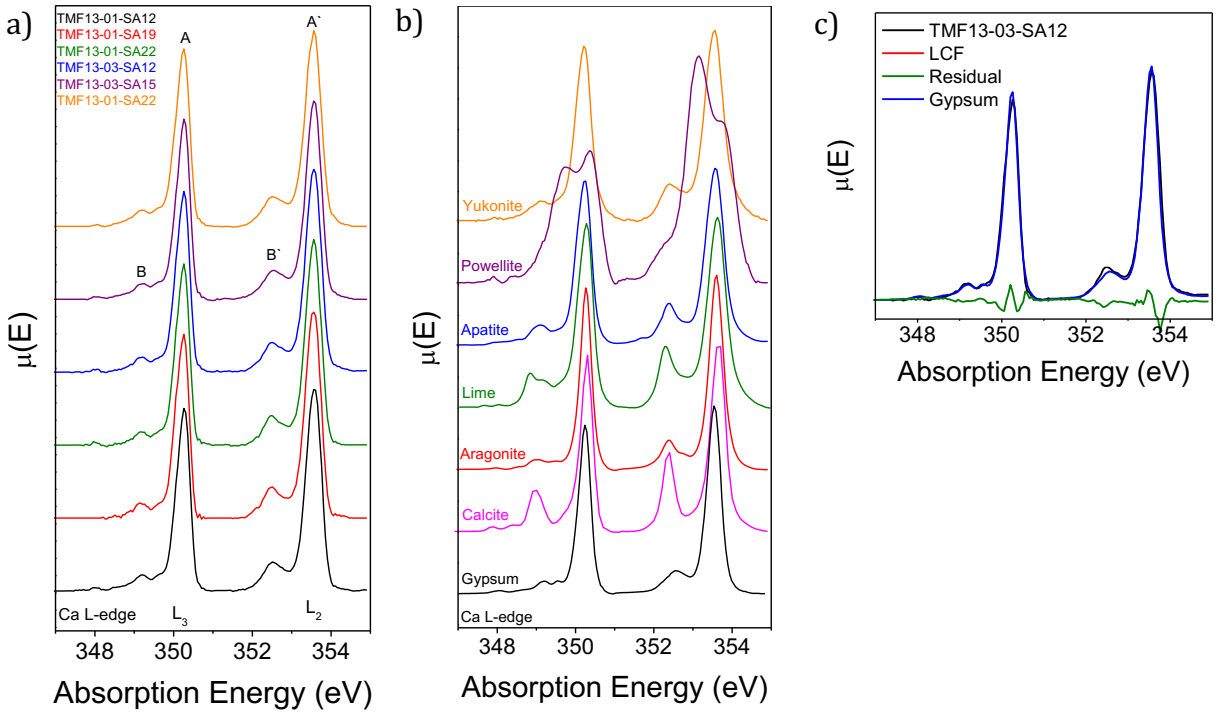

Figure 3. The bulk Ca $L_{2,3}$-edge XANES spectra from the a) tailings samples and b) calcium-containing standards are shown. Features A (A`) and B (B`) are discussed in the text. A comparison between the spectrum from tailings sample TMF13-03-SA12 and gypsum is presented in c).

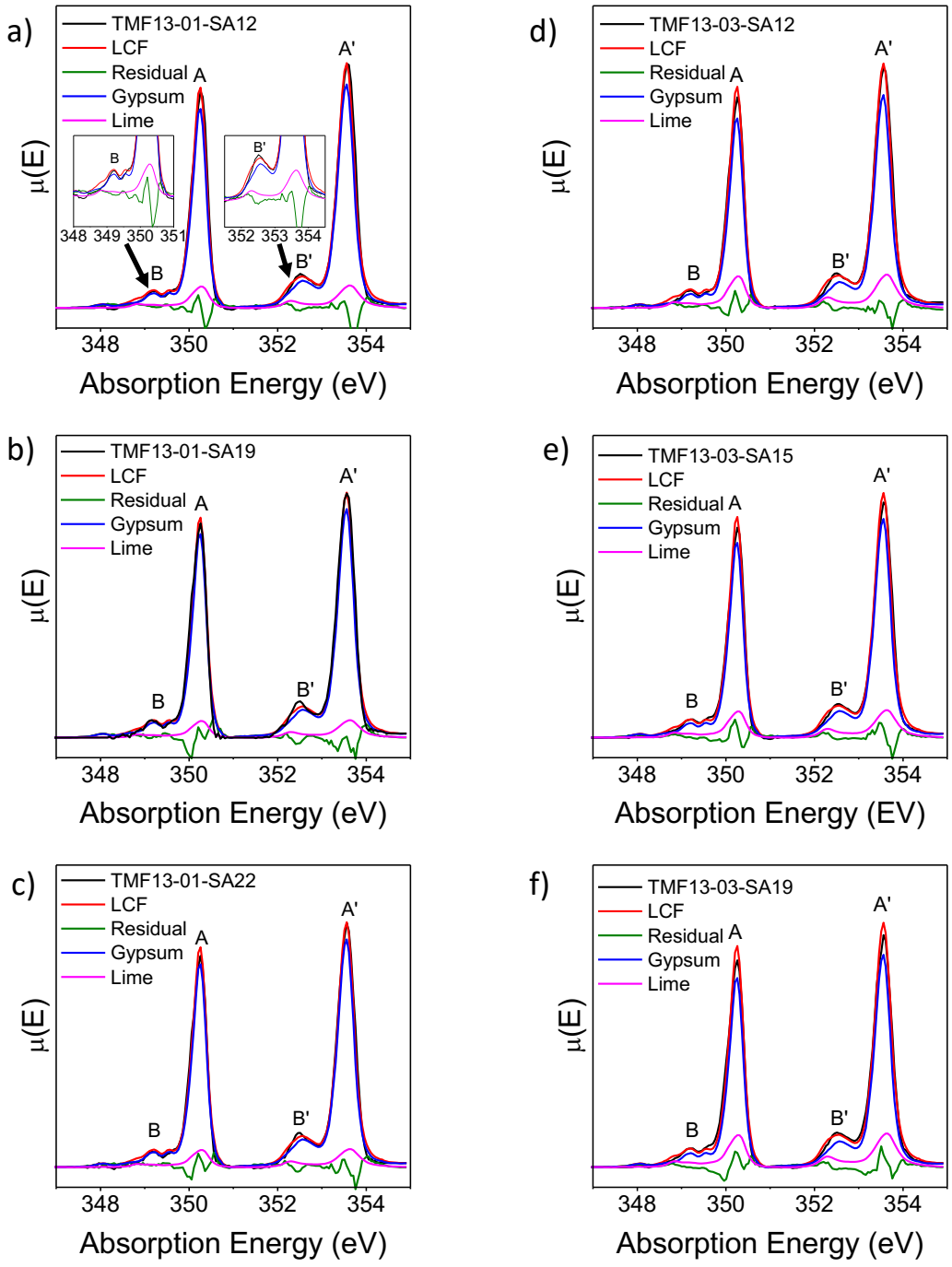

Figure 4. The fitted bulk Ca $L_{2,3}$-edge XANES spectra from a) TMF13-01-SA12, b) TMF13-01-SA19, c) TMF13-01-SA22, d) TMF13-03-SA12, e) TMF13-03-SA15, and f) TMF13-03-SA19. The linear combination fitting of each spectrum is shown in red and the residual is shown in green. The weighted spectra from the gypsum and lime are also shown. Note that similar fits were obtained when fitting the spectra to gypsum and other calcium-containing mineral species (see Figure S12). The inset of Figure 4(a) shows the intensity differences of features B and B' when comparing the tailings samples to gypsum.

Table 2. LCF results for the fitting of the bulk Ca $L_{2,3}$-edge XANES spectra from the tailings samples. Calculated errors are in brackets.

Sample	Gypsum (at%)	Lime* (at%)	R-factor	χ^2
TMF13-01-SA12	91(2)	9(3)	0.00832	264
TMF13-01-SA19	93(2)	7(6)	0.00962	299
TMF13-01-SA22	93(2)	7(6)	0.00652	194
TMF13-03-SA12	89(3)	11(2)	0.00521	153
TMF13-03-SA15	87(2)	13(3)	0.00685	192
TMF13-03-SA19	87(2)	13(2)	0.00701	193

* Similar results were obtained when fitting the spectra of the tailings samples to calcite, aragonite, powellite, or yukonite.

3.2.3 Bulk C K-edge XANES

The bulk Ca K/$L_{2,3}$-edge XANES analyses indicated that gypsum and possibly anhydrite are the most abundant calcium-containing mineral species in the JEB TMF. If present, the concentration of calcium carbonate is likely significantly lower than that of gypsum and would not be expected to contribute significantly to the lineshapes of the bulk Ca K/$L_{2,3}$-edge spectra. The C content of the TMF is relatively small, with organic and inorganic C accounting for less than 2.1 wt% and 0.4 wt%, respectively, of the total solid content of the tailings samples (see Table S2 in the SI). Therefore, calcium carbonate may be more observable in the bulk C K-edge spectra if it is present in the TMF at all. The bulk C K-edge XANES spectra of the tailings samples and some C-containing standards are shown in Figure 5. The standards presented were chosen to show the differences between C K-edge XANES spectra collected from organic vs. inorganic C species. The C K-edge corresponds to a dipole-allowed transition of a 1s electron to 2p states. Features corresponding to the K $L_{2,3}$-edge (~298 eV and ~300.5 eV) were also observed in the spectra as K is found in several of the clay minerals (i.e., sericite, smectite)

present in the tailings (Ahmet et al., 2012). Two major features are present in the C K-edge XANES spectra (see Figure S13). The first feature corresponds to a C 1s → π* transition (Cooney and Urquhart, 2004; Yabuta et al., 2014). This feature is observed at higher energies in carbonates (i.e., calcite; 290.4 eV) compared to hydrocarbon standards (i.e., kerosene; 284.9 eV). The shift in energy is due to the higher electronegativity of O compared to C (Allred and Rochow, 1958; Solomon et al., 2005). The second feature in the C K-edge corresponds to a C 1s → σ* transition (>288 eV). Multiple peaks are observed in this region of the C K-edge of carbonate species due to the interaction of carbon σ* states with next-nearest neighbour states (i.e., Ca 4p states). Broadening of this region in the C K-edge spectrum from kerosene may be due to multiple overlapping σ* transitions (i.e., C–C, C–H) as kerosene consists of a mixture of multiple hydrocarbon species (Cody et al., 1995).

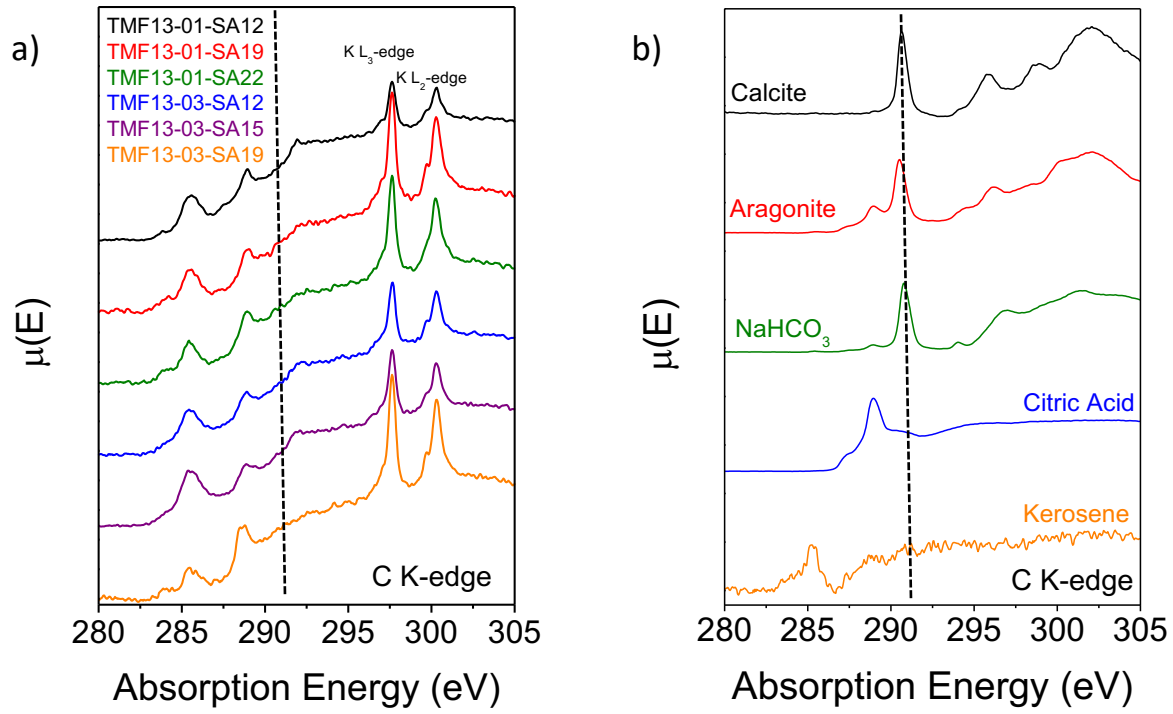

Figure 5. The bulk C K-edge XANES spectra from the a) tailings samples and b) carbon standards are shown. Peaks corresponding to the K $L_{2,3}$-edge were observed in the tailings samples due to the presence of K-containing clay minerals. The vertical dashed lines mark the location of the most distinguishable feature in C K-edge spectra from inorganic C species.

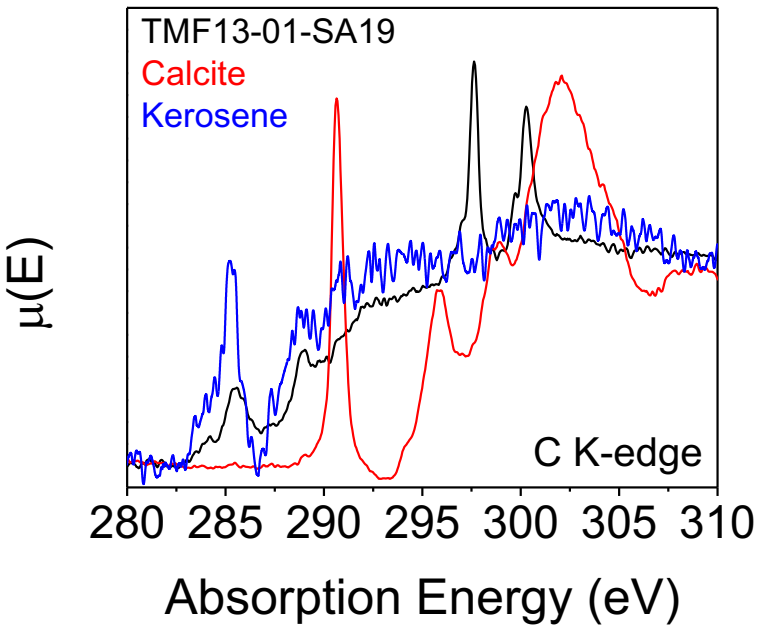

Figure 6. A comparison of the C K-edge XANES spectra from tailings sample TMF13-01-SA19 (black), carbonate (red), and kerosene (blue). Features in the C K-edge XANES spectrum from the tailings sample are more similar to those observed in organic C compounds than those observed in inorganic C compounds.

As shown in Figure 6, the bulk C K-edge spectra from the tailings samples appear to have a similar lineshape to that of kerosene. The most significant conclusion from this analysis is that the characteristic feature of carbonates (i.e. the C=O π* transition) was not observed in the spectra from the tailings samples, indicating that carbonates are not the major C-containing species in the TMF.

3.3 X-ray microprobe XRF mapping and Ca K-edge μ-XANES

The bulk XANES analyses indicated that the major Ca and C species in the TMF were gypsum and organic carbon, respectively, with no specific evidence of Ca-containing carbonate minerals being present in the TMF. If calcium carbonates are present in the tailings, the concentrations may be below the detection limits of the bulk XANES spectra collected from finely powdered samples using a large X-ray spot size. As evident from the μ-XRD study, a smaller X-ray beam

size (i.e., μm-size) focused on specific regions of individual grains of the samples can identify minor mineral species. Coupling μ-XANES with element-specific microprobe XRF maps was hypothesized to provide greater sensitivity to minor Ca-containing mineral species compared to both XRD and bulk XANES. Microprobe XRF maps and μ-XANES spectra were collected from three tailings samples (TMF13-01-SA19, TMF13-01-SA22, and TMF13-03-SA22) using a 10 μm X-ray beam size. The XRF maps collected from sample TMF13-01-SA19 are shown in Figure 7. All other soft X-ray XRF maps are shown in the SI (Figures S14 – S16). Two sets of XRF maps were collected from tailings sample TMF13-01-SA19 of different sizes; 500 x 500 μm and 1000 x 1000 μm. There is generally a strong correlation between Ca and S in all three tailings samples, consistent with the presence of calcium sulfate minerals (i.e., gypsum and anhydrite). A few Ca-rich regions with no correlating S-rich regions were observed in the XRF maps collected from tailings sample TMF13-01-SA19 (see Figure 7 and Figure S14 in the SI).

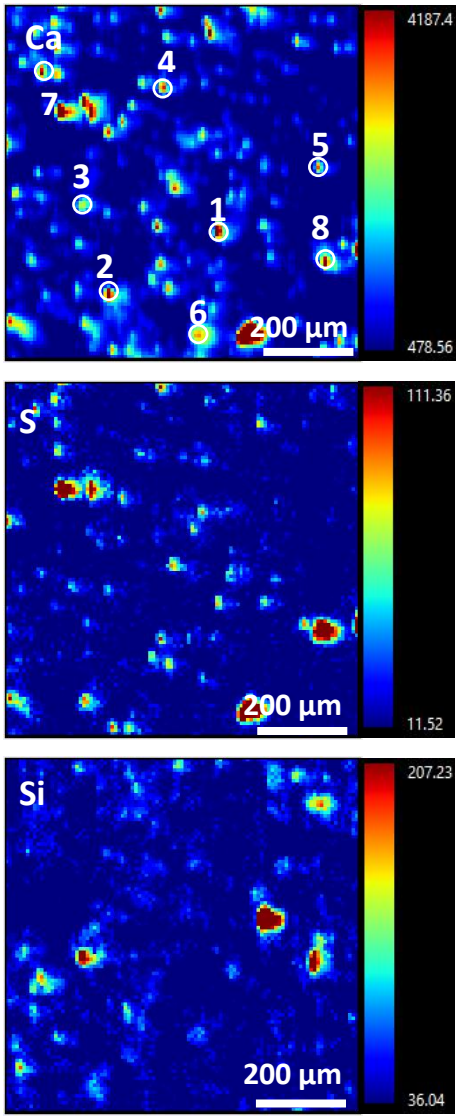

Figure 7. XRF maps showing the distribution of calcium (top), sulfur (middle), and silicon (bottom) collected from tailings sample TMF13-01-SA19. The size of the map was 1000 um x 1000 µm. Locations where Ca K-edge µ-XANES spectra were collected are marked on the Ca XRF map.

Ca K-edge µ-XANES spectra were collected from various locations of the XRF maps and are shown in Figures 8 and 9. The locations of where the spectra were collected from are marked on the calcium XRF maps (see Figure 7 and Figures S14 – S16 in the SI). Compared to the bulk Ca K-edge XANES spectra, there is a greater degree of lineshape variation in the µ-XANES spectra (see Figure S17 in the SI), with some having lineshapes that are considerably

different from that of gypsum or anhydrite. Several spectra collected from tailings sample TMF13-01-SA19 have lineshapes that are similar to calcite and dolomite (see Figures 8 and 9), suggesting that calcium carbonate minerals are present in the tailings.

A LCF analysis was performed on the μ-XANES spectra and the results of the LCF are shown in Table 3 and Table 4. Representative fitted Ca K-edge μ-XANES spectra are shown in Figure 10. All other fitted Ca K-edge μ-XANES spectra are shown in the SI (Figures S18 – S21). Only the fits having the lowest R-factor and χ^2 values are presented. In general, the Ca K-edge μ-XANES spectra were best fitted to one or two components. Most fitted μ-XANES spectra were found to contain gypsum and/or anhydrite, which is consistent with the bulk Ca K-edge XANES analysis. However, several other Ca-containing mineral species were also identified. Specifically, several μ-XANES spectra collected from the tailings samples were fitted to calcite, aragonite, or dolomite (see Figure 10 and Figures S18 – S19 in the SI). Tremolite ($Ca_2Mg_{4.5}Fe_{0.5}Si_6O_{22}(OH)_2$) was also identified in several μ-XANES spectra (see Figures S18a,d – S19c in the SI), suggesting that calcium magnesium silicate minerals are also present in the tailings. These mineral species appear to be present in the TMF at low concentrations because they were not identified by analysis of the bulk XANES spectra. The wide distribution of the species identified in the tailings, and the concentrations of these species listed in Tables 3 and 4, highlight the heterogeneous nature of the tailings and the considerable variability in composition between tailings samples collected at different locations in the TMF.

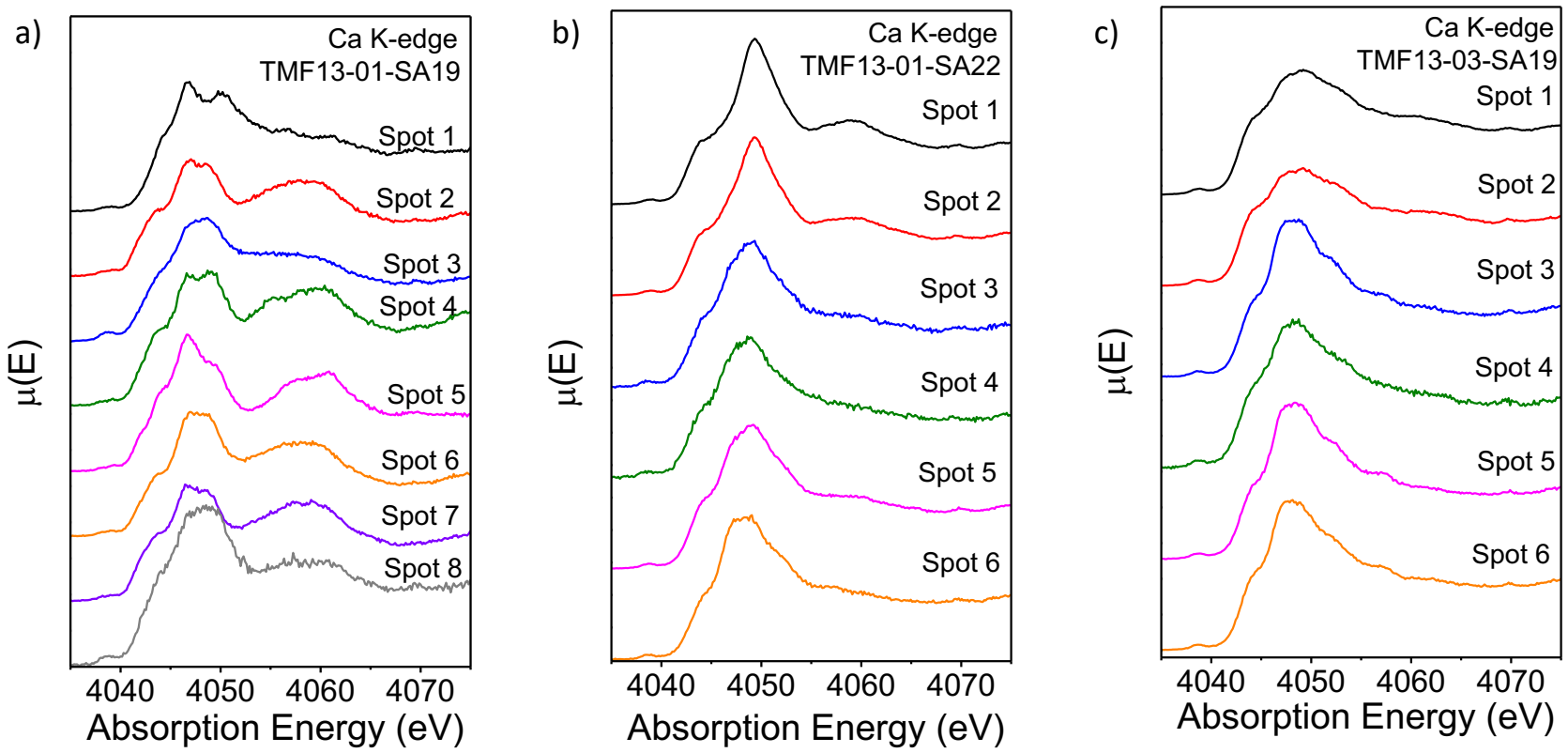

Figure 8. The Ca K-edge μ-XANES spectra collected from tailings samples a) TMF13-01-SA19, b) TMF13-01-SA22, and c) TMF13-03-SA19. Spectra were collected from the locations marked on the Ca XRF maps shown in Figure 7 (TMF13-01-SA19), Figure S15 (TMF13-01-SA22), and Figure S16 (TMF13-03-SA19).

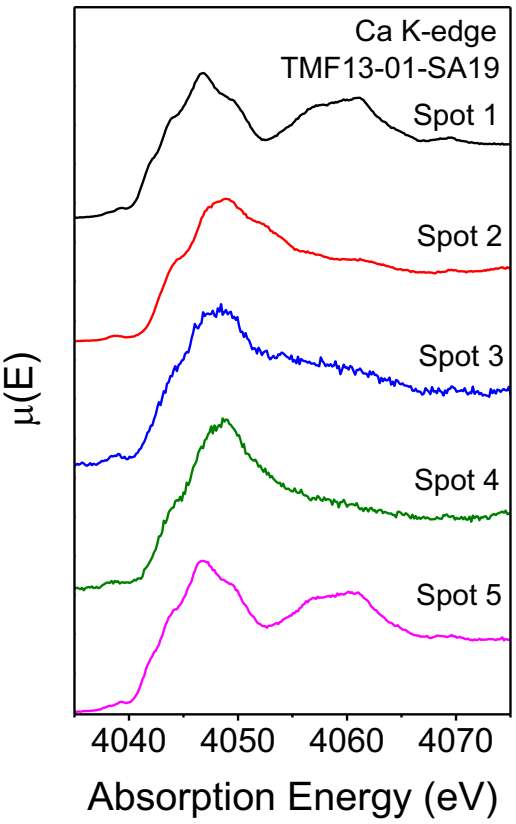

Figure 9. Ca K-edge μ-XANES spectra collected from tailings sample TMF13-01-SA19. Spectra were collected from specific positions that are marked on the Ca XRF map shown in Figure S14.

Table 3. LCF results for the fittings of the Ca K-edge μ-XANES spectra of the tailings samples. Calculated errors are in brackets.

Sample	Spot	Gypsum (at%)	Anhydrite (at%)	Calcite (at%)	Aragonite (at%)	Dolomite (at%)	Tremolite (at%)	R-factor	χ^2
TMF13-01-SA19[a]	1[b]								
	2			100				0.00711	0.779
	3	18(3)					82(5)	0.00550	0.397
	4	22(2)		78(3)				0.00614	0.433
	5					100		0.00604	0.479
	6			100				0.0165	1.21
	7			100				0.00525	0.391
	8	44(3)					56(5)	0.0163	1.124

[a] Spectra were collected from locations marked on the calcium XRF map shown in Figure 7.
[b] Spectrum could not be fitted to any of the calcium-containing standards used in this analysis.

Table 4. LCF results for the fittings of the Ca K-edge μ-XANES spectra of the tailings samples. Calculated errors are in brackets.

Sample	Spot	Gypsum (at%)	Anhydrite (at%)	Calcite (at%)	Aragonite (at%)	Dolomite (at%)	Tremolite (at%)	R-factor	χ^2
TMF13-01-SA19[a]	1					100		0.0124	1.07
	2	42(2)	58(3)					0.00362	0.307
	3	22(2)					78(2)	0.00991	0.740
	4	51(3)			49(3)			0.00789	0.759
	5					100		0.0105	0.975
TMF13-01-SA22[b]	1	100						0.0324	2.43
	2	100						0.0105	1.01
	3	89(3)			11(3)			0.00528	0.485
	4	39(2)			61(2)			0.00400	0.354
	5	91(3)			9(3)			0.00563	0.452
	6	100						0.0225	2.282
TMF13-03-SA19[c]	1	32(3)	68(3)					0.00448	0.390
	2	28(2)	82(2)					0.00461	0.375
	3	51(5)	49(4)					0.0142	1.46
	4	37(1)			63(2)			0.00292	0.264
	5	53(4)	48(3)					0.0117	1.24
	6	41(3)	59(3)					0.00858	0.890

[a] Spectra were collected from locations marked on the calcium XRF map shown in Figure S14.
[b] Spectra were collected from locations marked on the calcium XRF map shown in Figure S15.
[c] Spectra were collected from locations marked on the calcium XRF map shown in Figure S16.

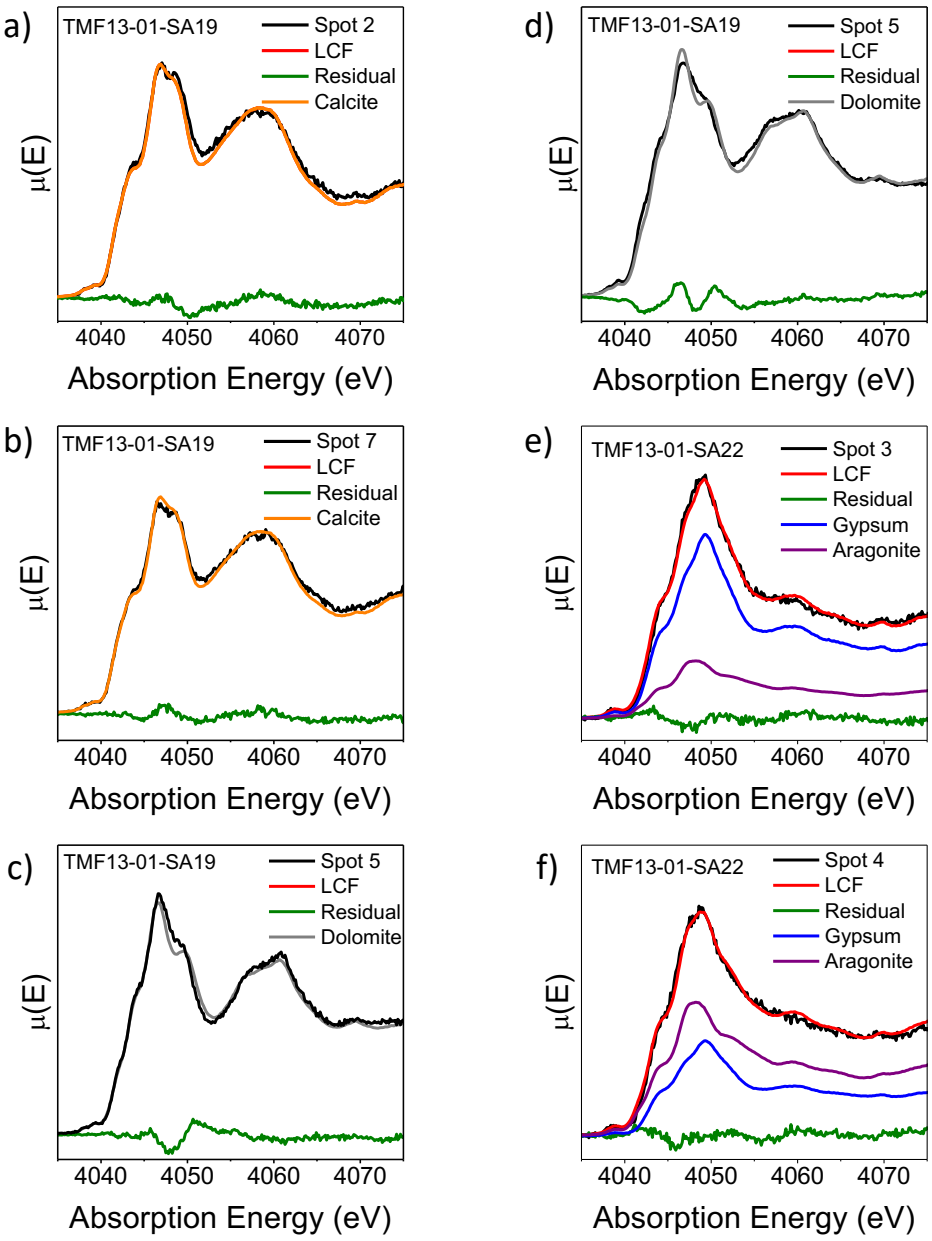

Figure 10. The fitted Ca K-edge μ-XANES spectra from a) TMF13-01-SA19 (collected from Spot 2 in Figure 5), b) TMF13-01-SA19 (collected from Spot 7 in Figure 5), c) TMF13-01-SA19 (collected from Spot 5 in Figure 7), d) TMF13-01-SA19 (collected from Spot 5 in Figure S14), e) TMF13-01-SA22 (collected from Spot 3 in Figure S15), and f) TMF13-01-SA22 (collected from Spot 4 in Figure S15) are shown. Note that μ-XANES spectra were collected from two different XRF maps of tailings sample TMF13-01-SA19. The linear combination fitting of each spectrum is shown in red and the residual is shown in green. The weighted standard spectra used to the fit the spectra are also shown.

It should be noted that the region in the Ca K-edge between 4045 - 4050 eV could not be fitted in some of the Ca K-edge μ-XANES spectra (see Figures S20d and S21c,e,f in the SI for examples). Also, the Ca K-edge μ-XANES spectrum collected from spot 1 from sample TMF13-01-SA19 (see Figure 8a) could not be fitted to any Ca-containing standards used in this analysis. This suggests that unknown calcium-containing mineral species may be present in the tailings, which further highlights the complexity of this system.

It is important to note that there are minor misfits in the near-edge region (i.e., 4040–4055 eV) of the Ca K-edge μ-XANES spectra fitted to dolomite (see Figures 10c,d and S19a in the SI for examples). Attempts to include a second component in these fittings were unsuccessful. Ideally, Ca^{2+} and Mg^{2+} cations are ordered in the dolomite structure with the Ca^{2+}:Mg^{2+} ratio close to 1:1 (i.e., $CaMg(CO_3)_2$) (Althoff, 1977). However, there is a small solid solution range in the dolomite structure (i.e., $Ca_{1-x}Mg_x(CO_3)_2$). Misfits in the near-edge region may be due to variations in the composition of dolomite forming in the TMF compared to the composition of the standard used in the LCF analysis. The LCF analysis of the μ-XANES spectra provides the first experimental evidence of the presence of calcium carbonates in the JEB TMF.

3.4 Electron microprobe

Although several Ca K-edge μ-XANES spectra collected were fitted to dolomite, it was not possible to confirm if Mg was present in the tailings solids from the microprobe analysis because the Mg Kα X-ray fluorescence energy (1253 eV) was below the detection limit of the detector used. Electron microprobe analysis was performed on several tailings samples to confirm the presence of Mg in the tailings. Backscattered electron (BSE) images and WDS maps (Ca, Mg, S, Si) collected from the tailings samples are shown in Figures S22 – S24 in the SI.

Bright spots in the BSE images correspond to regions of the tailings samples consisting of heavier elements. The WDS maps showed a strong correlation between Ca and S and between Mg and Si; however, multiple regions of the tailings were also observed to contain both Mg and Ca.

3.5 The formation of calcium-containing carbonate in the TMF

Calcite, aragonite, and dolomite were found to be present at low concentrations in samples collected from the TMF. Although calcite is the most thermodynamically stable form of calcium carbonate (Anderson and Crear, 1993), the stability of different forms of $CaCO_3$ is influenced by a number of factors such as temperature, pH, and dissolved salt content (Walter, 1986l; Burton and Walter, 1990; Cooke and Kepkay, 1980; Berner, 1975). However, pH and dissolved salt concentrations are the most likely factors influencing the formation of calcite and aragonite because the low temperature of the TMF (~+6 ^{o}C) will support the precipitation of both species (Mayer, 1984). Aragonite stabilizes at a pH greater than 7 whereas a lower pH supports the stabilization of calcite (Berner, 1975). Likewise, the presence of dissolved ions, such as SO_4^{2-}, Mg^{2+}, Mn^{2+}, and Fe^{2+} can inhibit the formation of calcite (Walter, 1986; Berner, 1975; Mayer, 1984; Dromgoole and Walter, 1990). Larger cations, such as Sr^{2+}, Ba^{2+}, and Pb^{2+}, can also stabilize aragonite because the larger unit cell of this mineral compared to calcite favours the incorporation of larger cations (Wray and Daniels, 1957). As shown in Table S3 in the SI, the pH of the pore water and the concentrations of many of the ions mentioned above vary throughout the TMF, which would be expected to influence the stability of calcite and aragonite.

The presence of dolomite in the TMF is surprising as hydration of Mg and dissolved salts prevents the ordering of Ca and Mg within the dolomite structure (Althoff, 1977; Folk and Land, 1975). However, dolomite is known to form in the marine environment due to the substitution of

dissolved Mg^{2+} into the calcite structure, forming a disordered magnesium calcite (Folk and Land, 1975; Katz and Matthews, 1977). The ordering of Ca and Mg cations in the calcite structure, particularly at elevated pressures, leads to the formation of dolomite (Althoff, 1977). Although the Mg^{2+} pore water concentration is significantly lower than that of Ca^{2+} (see Table S3), dolomite could form from the ordering of magnesium calcite containing less than 10 at% of Mg^{2+} (Katz and Matthews, 1977).

4. Conclusions

Tailings samples collected from the JEB TMF in 2013 were analyzed using X-ray diffraction and spectroscopy to determine if calcium-containing carbonates are present. This study demonstrated that μ-XANES analysis coupled with microprobe XRF mapping is the optimum technique for analysing low concentration calcium carbonates in the TMF. This combination of techniques identified several minor calcium-containing mineral species in the TMF, specifically the carbonate minerals of calcite, aragonite, and dolomite.

Current models of the geochemistry of the JEB TMF suggest that the precipitation of Ca-bearing carbonates by the reaction of aqueous bicarbonate and gypsum will control the concentration of aqueous bicarbonate in the tailings, and, as a result, will also control the concentration of soluble uranium carbonate complexes in the TMF. The precipitation of carbonate minerals should limit the ability of U to be exposed to the environment external to the TMF. The identification of calcite, aragonite, and dolomite in the tailings in this study has provided validity to this model, although further studies of how the concentration of Ca-bearing carbonates and U oxides in the TMF change with age will need to be completed before this model can be confirmed.

Acknowledgments

AREVA and NSERC are thanked for funding this research. CFI is thanked for providing funds to purchase the PANalytical Empyrean powder XRD used in this work. The authors extend their thanks to Ms. Aimee Maclennan, Dr. Youngfeng Hu, and Dr. Tom Regier for their help in carrying out measurements on the SXRMB and SGM beamlines at the CLS. The CLS is funded by NSERC, the Canadian Foundation of Innovation (CFI), the National Research Council (NRC), the Canadian Institutes of Health Research (CIHR), the Government of Saskatchewan, the Western Economic Diversification Canada, and the University of Saskatchewan. The Saskatchewan Research Council's Environmental Analytical Division is thanked for measuring pore water concentrations. M. R. Rafiuddin, E. R. Aluri, and J. R. Hayes (University of Saskatchewan) are thanked for their contributions.

References

Ahmed, A. A.; Kühn, O.; Leinweber, P. 2012. Controlled experimental soil organic matter modification for study of organic pollutant interactions in soil. *Sci. Total Environ. 441*, 151-158.

Allred, A. L.; Rochow, E. G. 1958. A scale of electronegativity based on electrostatic forces. *J. Inorg. Nucl. Chem. 5*, 264-268.

Althoff, P. L. 1977. Structural refinements of dolomite and a magnesian calcite and implications for dolomite formation in marine environments. *Am. Mineral.*, *62*, 772-783.

Anderson, G. M.; Crerar, D. A. 1993. Thermodynamics in geochemistry: The equilibrium model. Oxford University Press, New York.

AREVA Resources Canada Ltd. (AREVA) 2015. McClean Lake operation technical information document (TID): Tailings Management. Version 01. Revision 00. A copy of the report can be requested from AREVA Resources Canada (e-mail: publicrelations@areva.ca) or the Canadian Nuclear Safety Commission (http://nuclearsafety.gc.ca/eng/uranium/mines-and-mills/nuclear-facilities/mcclean-lake/index.cfm).

Beauchemin, S.; Hesterberg, D.; Beauchemin, M. 2002. Principal component analysis approach for modelling sulphur K-XANES spectra of humic acids. *Soil Sci. Soc. Am. J. 66*, 83-91.

Berner, R. A. 1975. The role of magnesium in the crystal growth of calcite and aragonite from sea water. *Geochim. Cosmochim. Acta*, *39*, 489-504.

Blanchard, P. E. R.; Hayes, J. R.; Grosvenor, A. P.; Rowson, J.; Hughes, K.; Brown, C. 2015. Investigating the geochemical model for molybdenum mineralization in the JEB Tailings Management Facility at McClean Lake, Saskatchewan: An X-ray absorption spectroscopy study. *Environ. Sci. Technol. 49*, 6504-6509.

Burton, E. A.; Walter, L. M. 1990. The role of pH in phosphate inhibition of calcite and aragonite precipitation rates in seawater. *Geochim. Cosmochim. Acta 54*, 797-808.

Cassinelli, W. H.; Martins, L.; Passos, A. R.; Pulcinelli, S. H.; Santilli, C. V.; Rochet, A.; Briois, V. 2014. Multivariate curve resolution analysis applied to time-resolved synchrotron X-ray absorption spectroscopy monitoring of the activation of copper alumina catalyst. *Catal. Today*. *229*, 114-122.

Chen, N.; Jiang, D. T.; Cutler, J.; Kotzer, T.; Jia, Y. F.; Demopoulos, G. P.; Rowson, J. W. 2009. Structural characterization of poorly-crystalline scorodite, iron(III)−arsenate co-precipitates and uranium mill neutralized raffinate solids using X-ray absorption fine structure spectroscopy. *Geochim. Cosmochim. Acta*, *73*, 3260−3276.

Cody, G. D.; Botto, R. E.; Ade, H.; Behal, S.; Disko, M.; Wirick, S. 1995. Inner-shell spectroscopy and imaging of a subbituminous coal: In-situ analysis of organic and inorganic microstructure using C(1s)-,Ca(2p)-, and Cl(2s)-NEXAFS. *Energy Fuels*, *9*, 525-533.

Cooke, R. C.; Kepkay, P. E. 1980. pH and water chemistry at one atmosphere. *Geochimica et Cosmochimica Acta*, *44*, 1071-1075.

Cooney, R. R.; Urquhart, S. G. 2004. Chemical trends in the near-edge X-ray absorption fine structure of monosubstituted and para-bisubstituted benzenes. *J. Phys. Chem. B*, *108*, 18185-18191.

De Groot, F. M. F.; Fuggle, J .C.; Thole, B. T.; Sawatzky, G. A. 1990. $L_{2,3}$ X-ray absorption edges of d^0 compounds: K^+, Ca^{2+}, Sc^{3+}, and Ti^{4+} in *Oh* (octahedral) symmetry. *Phys. Rev. B*, *41*, 928–937.

Dromgoole, E. L.; Walter, L. M. 1990. Inhibition of calcite growth rates by Mn^{2+} in $CaCl_2$ solutions at 10, 25, and 50 ^{o}C. *Geochim. Cosmochim. Acta*, *54*, 2991-3000.

Wray, J. L.; Daniels, F. 1957. Precipitation of calcite and aragonite. *J. Am. Chem. Soc.*, *79*, 2031-2034.

Fernández-Garcìa, M.; Márquez Alvarez, C.; Haller, G.L. 1995 XANES-TPR study of Cu – Pd bimetallic catalysts: application of factor analysis. *J. Phys. Chem. 99*, 12565–12569.

Hayes, J. R.; Grosvenor, A. P.; Rowson, J.; Hughes, K.; Frey, R. A.; Reid, J. 2014. Analysis of the Mo speciation in the JEB Tailings Management Facility at McClean Lake, Saskatchewan. *Environ. Sci. Technol. 48* 4460-4467.

Folk, R. L.; Land, L. S. 1975. Mg/Ca ratio and salinity: Two controls over crystallization of dolomite. *AAPG Bull.*, *59*, 60-68.

Himpsel, F. J.; Karlsson, U. O.; McLean, A. B.; Terminello, L. J.; de Groot, F. M. F.; Abbate, M.; Fuggle, J. C.; Thole, B. T.; Sawatzky, G. A. 1991. Fine structure of the Ca 2p X-ray absorption edge for bulk compounds, surfaces, and interfaces. *Phys. Rev. B 43*, 6899-6907.

Hu, Y. F.; Coulthard, I.; Chevrier, D.; Wright, G.; Igarashi, R.; Sitnikov, A.; Wates, B. W.; Hallin, E. L.; Sham, T. K.; Reininger, R. 2010. Preliminary commissioning and performance of the Soft X-ray Microcharacterization beamline at the Canadian Light Source. *AIP Conf. Proc. 1234*, 343-346.

Katz, A.; Matthews, A. 1977. The dolomitization of $CaCO_3$: an experimental study at 252-295 ^{o}C. *Geochim. Cosmochim. Acta*, , *41*, 297-308.

Kraus, W.; Nolze, G. 1996. POWDER CELL: A program for the representation and manipulation of crystal structures and calculation of the resulting X-ray powder patterns. *J. Appl. Crystallogr. 29*, 301−303.

Langmuir, D.; Mahoney, J.; Rowson, J. 2006. Solubility products of amorphous ferric arsenate and crystalline scorodite ($FeAsO_4 \cdot 2H_2O$) and their application to arsenic behaviour in buried mine tailings. *Geochim. Cosmochim. Acta 70*, 2942−2956.

Liu, L. J.; Liu, H. J.; Cui, M. Q.; Hu, Y. F.; Zheng, L.; Zhao, Y. D.; Ma, C. Y.; Xi, S. B.; Yang, D. L.; Guo, Z. Y.; Wang, J. 2013. Determination of the calcium species in coal chars by Ca K-edge XANES analysis. *Chinese Phys. C. 37*, 028003.

Mahoney, J.; Slaughter, M.; Langmuir, D.; Rowson, J. 2007. Control of As and Ni releases from a uranium mill tailings neutralization circuit: Solution chemistry, mineralogy and geochemical modeling of laboratory study results. *Appl. Geochem. 22*, 2758−2776.

Malinowski, E.R. 1977. Theory of error in factor analysis. *Anal. Chem. 49*, 606-612.

Malinowski, E. R. 2002. Factor Analysis in Chemistry, 3rd ed., John Wiley & Sons, New York.

Mayer, H. J. 1984. The influence of impurities on the growth rate of calcite. *J. Cryst. Growth*, , *66*, 639-646.

Politi, Y.; Metzler, R. A.; Abrecht, M.; Gilbert, B.; Wilt, F. H.; Sagi, I.; Addadi, L.; Weiner, S.; Gilbert, P. 2005. Transformation mechanism of amorphous calcium carbonate into calcite in the sea urchin larval spicule. *Proc. Natl. Acad. Sci. 105*, 17362-17366.

Ravel, B.; Newville, M. 2005. ATHENA, ARTEMIS, HEPHAESTUS: data analysis for X-ray absorption spectroscopy using IFEFFIT. *J. Synchrotron Rad. 12*, 537-541.

Regier, T.; Krochak, J.; Sham, T. K.; Hu Y. F.; Thompson, J.; Blyth, R. I. R. 2007. Performance and capabilities of the Canadian Dragon: The SGM beamline at the Canadian Light Source. *Nucl. Instrum. Meth. A 582*, 93-95.

Rehr, J. J. 2000. Theoretical approaches to X-ray absorption fine structure. *Re. Mod. Phys. 72*, 621-654.

Solomon, D.; Lehmann, J.; Kinyangi, J.; Liang, B.; Schäfer, T. 2005. Carbon K-edge NEXAFS and FTIR-ATR spectroscopy investigation of organic carbon speciation in soils. *Soil Sci. Soc. Am. J.*, *69*, 107-119.

Sowrey, F. E.; Skipper, L. J.; Pickip, D. M.; Drake, K. O.; Lin, Z.; Smith, M. E.; Newport, R. J. 2004. Systematic empirical analysis of calcium-oxygen coordination environment by calcium K-edge XANES. *Phys. Chem. Chem. Phys. 6*, 188-192.

Takahashi, Y.; Miyoshi, T.; Yabuki, S.; Inada, Y.; Shimizu, H. 2008. Observation of transformation of calcite to gypsum in mineral aerosols by Ca K-edge X-ray absorption near-edge structures (XANES). *Atmos. Environ. 42*, 6635-6541.

Walter, L. M. 1986. Relative efficiency of carbonate dissolution and precipitation during diagenesis: *Roles of organic matter in sediment diagenesis. 38*, 1-11.

Webb, S. M. 2011. The MicroAnalysis Toolkit: X-ray fluorescence image processing software. *AIP Conf. Proc. 196*, 196−199.

Yabuta, H.; Uesugi, M.; Naraoka, H.; Ito, M.; Kilcoyne, A. L. D. Sandford, S. A. Kitajima, F.; Mita, H.; Takano, Y.; Yada, T.; Karouji, Y.; Ishibashi, Y.; Okada, T.; Abe, M. 2014. X-ray absorption near edge structure spectroscopic study of Hayabusa category 3 carbonaceous particles. *Earth Planets Space*, *66*, 156.